RSC Advances

ROYAL SOCIETY OF CHEMISTRY

www.rsc.org/advances

Magnetic Properties of Corrosion-Resistant CoW Films

Lina Yu [a], Liying Lu [b,*], Zedong Xu [a], Jianjun Ma [a], Min Gao [a], Xiaoguang Xu [a], Yong Jiang [a,*]

a. State Key Laboratory for Advanced Metals and Materials, School of Materials Science and Engineering, University of Science and Technology Beijing, Beijing, 100083, China

b. School of Chemistry and Biological Engineering, University of Science and Technology Beijing, Beijing, 100083, China

Abstract

CoW films with different compositions have been prepared by an electrochemical deposition method. The tungsten contents in the CoW films are controlled through adjusting electrolyte concentrations, pH values and applied potentials. The magnetic and corrosion-resistant properties of the CoW films are systematically studied. With the increase of tungsten contents and the annealing temperature, the CoW films transfer from in-plane magnetic anisotropy to magnetic isotropy, which is related to the formation of hexagonal close packed (*hcp*) Co_3W phase confirmed by the morphological and phase evolution. The magnetic properties of CoW films can maintain stable even after having been immersed in a 0.5% NaCl solution for 170 hours. A ultrathin tungsten oxide passivation layer is found on the surface of the films which can protect CoW film from corrosion.

Keywords: CoW alloys, electrochemical deposition, magnetic property, corrosion resistance

* Corresponding authors. Tel. /fax: +86 10 62333209.
E-mail addresses: luly@ustb.edu.cn(L.Y. Lu), yjiang@ustb.edu.cn(Y. Jiang)

1. Introduction

There are big challenges on materials' design, development and commercialization to explore multifunctional materials with excellent overall performance and low cost fabrication process. CoW alloys are the kinds of materials combining outstanding magnetic, catalytic and corrosion resistance properties with excellent mechanical performance, attracting great attentions in many fields including recording media, micro-electro-mechanical systems (MEMS) and catalysts for clean hydrogen generation from water decomposition.[1-4] Typically, CoW alloys are prepared by an electrochemical deposition method, which is a well-developed technology to fabricate films with controllable composition and microstructure in an easy operational way. Compared with physical deposition method such as magnetron sputtering, electrodeposited process is more economic.[5] Furthermore, the composition, morphology and properties of CoW films can be controlled by adjusting electrodeposition parameters.[6] Although tungsten atoms cannot be electrodeposited from aqueous solution by itself due to their low deposition potential, co-deposition of tungsten and cobalt can take place when cobalt salts are also added to electrolyte solutions. In this "induced co-deposition" process, cobalt atoms act as catalysts for the deposition of tungsten.[7] Many theories have been proposed to explain this anomalous co-deposition process, but none of them has been fully proven and accepted. Since there are organic additives in electrolyte solutions, a complex species model is adopted here, which considers the iron-group metal tungstate complexes as precursors to electrodeposit tungsten alloys.[8, 9] Varying the depositional condition, CoW alloys with different compositions, morphologies and thus tailored magnetic properties can be obtained. In particular, the hexagonal close packed (*hcp*) Co_3W films with (001) texture exhibit perpendicular-to-plane magnetic anisotropy, which is promising as next magnetic storage media.[10]

The as-deposited CoW alloys are not well crystallized or even amorphous, which have unsatisfied performance in not only magnetism but also mechanical and corrosion aspects.[11] A post heat treatment process is needed to improve their overall performance for their applications in various conditions.[12] However, effects of compositions and phase structures evolution on the magnetic properties of CoW alloy films have not been systematically studied yet, all of which are worth to be explored in detail to understand the involved mechanism and realize their reliable usage in various conditions. So it is critical to study the magnetic properties of CoW alloy films with different composition, annealing processes and the corrosion environment. In this paper, we dedicate to optimize the electrodeposition and subsequent annealing process to obtain CoW alloy films with better and stable overall performance.

2. Experimental

The CoW films were deposited by using a DC potentiostatic method. The electrochemical deposition was performed in a conventional three-electrode cell with Ag/AgCl electrode, platinum electrode and copper foil as the reference, counter and working electrodes, respectively. Copper substrates were cut into 12×50 mm^2 and annealed at 400 °C in vacuum for 30 min for internal stress relief. Then copper substrates were cleaned with acetone and activated by 1 $mol \cdot L^{-1}$ H_2SO_4 solution. The basic electrolyte solution contained 0.1 $mol \cdot L^{-1}$ of $CoSO_4$, 0.5 $mol \cdot L^{-1}$ of Na_2WO_4, 0.2 $mol \cdot L^{-1}$ of sodium citrate (Na_3Cit). Citric acid was chosen to adjust pH values and then sodium citrate/citric acid were also used as buffer solution, which can stabilize the pH value. No inorganic impurity can enter CoW films during electrodeposition process.

The as-prepared CoW alloy films were annealed in vacuum (< 5.0×10^{-5} Pa) for 30 minutes. The samples were then characterized by a leo-1450 scan electron microscopy with energy

dispersive spectroscopy (SEM-EDS), M21X X-ray diffraction (XRD), physical property measurement system (PPMS), and Kratos AXIS ULTRA DLD X-ray photoelectron spectroscopy (XPS) to determine their compositions, morphologies, crystal structures, magnetic properties and chemical valence of elements at room temperature, respectively.

3. Results and discussion

The properties of CoW films greatly depend on the quality of films, which is decided by electrodeposition parameters including pH values, electrolyte concentrations and applied potentials. Figure 1 shows the cyclic voltammograms for the solutions with different pH values. The pH values are adjusted as 6.0, 6.5, 8.0 through adding citric acid in the basic electrolyte. In order to make the peaks in curves more obvious, current (I) on cyclic voltammograms is converted into log (I). It can be observed that each curve for acid solutions has only one reduction peak, which is between -0.7 V and -0.8 V. Different from acid solutions, two peaks appear during the reduction process when the pH value of 8.0 is adopted. The peak at the potential of -0.7 V corresponds to the reduction of Co^{2+}, and the other one near -0.3 V indicates the formation of metal oxides. In fact, the forms of Co^{2+} and WO_4^{2-} are rather complicated, which highly depends on the pH values and the concentration ratio of Co^{2+} and WO_4^{2-}.[7] In these experiments, the main forms of Co^{2+} are $[(Co)(Cit)]^-$ and $[(Co)(Cit)_2]^{4-}$, and WO_4^- ions exist as $[(WO_4)(Cit)(H)_2]^{3-}$ and $[(WO_4)(Cit)(H)]^{4-}$. The $[(Co)(Cit)]^-$ can further complex with $[(WO_4)(Cit)(H)]^{4-}$ to form $[(Co)(WO_4)(Cit)(H)]^{2-}$ which is the only precursor that tungsten can be deposited from. Cobalt itself can also be deposited in a parallel route from $[(Co)(Cit)]^-$. The main complexes are formed and reduced as below reactions.

$$Co^{2+} + Cit^{3-} \rightarrow [(Co)(Cit)]^- \quad (1)$$

$$Co^{2+} + 2Cit^{3-} \rightarrow [(Co)(Cit)_2]^{4-} \quad (2)$$

$$WO_4^{2-} + Cit^{3-} + H^+ \rightarrow [(WO_4)(Cit)(H)]^{4-} \quad (3)$$

$$WO_4^{2-} + Cit^{3-} + 2H^+ \rightarrow [(WO_4)(Cit)(H)_2]^{3-} \quad (4)$$

$$[(Co)(Cit)]^- + [(WO_4)(Cit)(H)]^{4-} \rightarrow [(Co)(WO_4)(Cit)(H)]^{2-} + Cit^{3-} \quad (5)$$

$$[(Co)(Cit)]^- + 2e^- \rightarrow Co + Cit^{3-} \quad (6)$$

$$[(Co)(WO_4)(Cit)(H)]^{2-} + 8e^- + 3H_2O \rightarrow CoW + 7OH^- + Cit^{3-} \quad (7)$$

The exact deposition parameters for CoW films with different W content are shown in Table 1. The tungsten contents in the CoW films increased by increasing the pH values, which are 11, 14, 17 and 19 at.% W for pH 6.0, 6.5, 7.0, 8.0, respectively. This result is reasonable because the cobalt deposition is facilitated by the formation of $[(Co)(Cit)]^-$ species in a near neutral electrolyte. However, with the increasing pH values, more cobalt ions tend to form cobalt hydroxide, which inhibits the deposition of cobalt atoms and increases the tungsten content in films.[13] For the potential-dependent experiment, the basic electrolyte solution with pH 6.5 is adopted. The tungsten contents in the deposited CoW films are 26, 15 and 9 at.% W when the deposition potentials are -1.0, -1.5 and -2.0 V, respectively. With high current density, which is proportional to the applied potential, the co-deposition exhibits a mass transport control rather than a kinetic one.[14] Since there is no rotation device to accelerate the diffusion, a lower deposition potential is beneficial to the deposition of small complex with a higher diffusion coefficient, thus the enhancement of the deposition rate of cobalt atoms is more obvious than that of tungsten atoms. The influence of the concentration of Na_2WO_4 on the compositions of CoW films is also studied. It is observed that the CoW films with 14, 17, 18, 20, 20 at.% W are

produced by 0.05, 0.1, 0.2, 0.3 and 0.4 mol·L^{-1} Na_2WO_4, respectively. Generally, the tungsten content increases with the concentration of Na_2WO_4 below 0.3 mol·L^{-1}. The increase of the WO_4^{2-} concentration in electrolyte facilitates the formation of cobalt-tungstate complex at the beginning of electrodeposition, causing the tungsten content in CoW films rising. However, when the WO_4^{2-} concentration is further increased to 0.4 mol·L^{-1}, the tungsten content keeps constant, even decrease slightly. Because Cit^{3-} is insufficient to form the $[(Co)(Cit)_2]^{4-}$ complex, a simpler complex $[(Co)(Cit)]^-$ is preferred from which cobalt can be deposited more readily, resulting in relatively increased cobalt content.

The effect of composition on phase structure of CoW films is studied by XRD, as shown in Fig. 2a. All the CoW films are annealed at 600 °C for 30 min in vacuum. It can be observed that the CoW film with 2 at.% W has a structure similar to pure *hcp*-Co because tungsten atoms prefer to diffuse into the crystal lattice of *hcp*-Co and form a solid solution when the tungsten content is very few. However, the solubility of tungsten atoms in cobalt matrix is very limited due to their high difference in atom radius (r_{Co}=125 pm, r_W=141 pm). Further increasing the tungsten content could destroy the solid solution structure and make tungsten atoms segregate, forming a W-rich metallic phase at the Co-rich solid boundaries preferred by surface energy.[3] For the CoW film with 18 at.% W, the diffraction peaks of *hcp*-Co_3W alloy phase begin to appear at 40.56 °, 43.66 ° and 46.29 °, which correspond to (100), (002) and (101) planes, respectively. When the tungsten content in the CoW films gradually rises to 26 at.%, more tungsten atoms incorporate into the lattice causing further expansion of the crystal lattice, and therefore all diffraction peaks shift to lower 2θ angles. All the diffraction peaks can well index to CoW phase without any distinct tungsten oxides peak.

The CoW films with 26 at.% W(expressed as Co_3W films in later sections) are annealed at different temperatures and then used to study the crystallization process of hcp-Co_3W phase by XRD. As shown in Fig. 2b, the as-prepared and 500 °C annealed Co_3W films have no diffraction peaks. After annealed at 550 °C, the (100), (002) and (101) peaks of the *hcp*-Co_3W appear. And all diffraction peaks further sharpen and intensify when the annealing temperature rises to 600 °C and 650 °C. With increasing the annealing temperature, the (100) peak at $2\theta=40.56^{o}$ shifts obviously towards a lower 2θ angle. Calculation results show that the *a*-axis lattice constant increases with the increased annealing temperature, while the *c*-axis lattice constant increases from 550 °C to 600 °C and slightly decreases for the 650 °C annealed film.

The morphological evolution of the annealed Co_3W films is observed by SEM, as shown in Fig. 3a-e. Fig. 3f is the EDS result of the Co_3W films. The as-deposited and 500 °C annealed Co_3W films are almost homogeneous, as in Fig. 3a and b, respectively. This agrees with the reported results that the alloys with high tungsten content have small grain size.[15] The Co_3W films annealed at 550 ºC begin to crystallize. A few tiny surface cracks show up due to the stress between the Co_3W film and the copper substrate for their mismatched thermal expansion coefficients. When the annealing temperature increases to 600 ºC, the Co_3W grains continue to grow up and the crystalline structure becomes better. Compared with the 600 ºC annealed one, the Co_3W film annealed at 650 ºC becomes more compact. The results are consistent with the XRD measurement.

The magnetic properties of the CoW films with different tungsten contents annealed 600 °C for 30 min in vacuum are measured at room temperature by PPMS, as shown in Fig. 4a-e. The dependence of in-plane magnetic coercivity (H_C) on the tungsten content of the CoW films has a

clear transition point at 11 at.% W, as shown in Fig. 4f. When the tungsten content is less than 11 at.%, the H_C of the CoW films decreases with the increased tungsten content. It is due to the random replacement of cobalt atomic positions with nonmagnetic tungsten atoms in lattices, which destroys exchange coupling among cobalt domains and makes magnetic moment be easily reversed. When the tungsten content in the CoW films further increases, H_C increases due to the gradually formed Co_3W phase with hard ferromagnetic property. For the in-plane remanence ratio (M_r/M_S) curve of the CoW films shown in Fig. 4f, it firstly decreases and then increases when the tungsten content exceeds 11 at. %. M_r/M_S decreases again when the tungsten content is beyond 20 at. %. It is known that the pure Co phase has a larger M_r/M_S value since the magnetic energy level of the pure Co phase is higher than that of Co_3W. At the beginning, the nonmagnetic W atoms enter the Co lattice and dilute the magnetic moment of Co atoms, which leads to a reduction of M_r/M_S values. When the tungsten content is beyond 11 at.%, tungsten atoms tend to segregate at the grain boundaries and Co_3W phase forms, which results in the mixture of Co and Co_3W phases in the films. Dominated by the pure Co phase, M_r/M_S turns to increase with the tungsten content. However, the *hcp*-Co_3W phase becomes the main phase when the tungsten content is beyond 20 at.%. Because the *hcp*- Co_3W phase is a hard magnetic phase with lower M_r/M_S value than Co, M_r/M_S decreases with increasing tungsten content. Therefore the magnetic properties are contributed to the evolution of composition and crystal structure in the films, which is consistent with the XRD results in Fig. 2. It can also be observed that the CoW films transfer from in-plane magnetic anisotropy to magnetic isotropy with increasing tungsten content. According to the XRD results in Fig. 2a, the transformation of magnetic anisotropy seems to be related to the formation of *hcp*-Co_3W phase.

In Fig. 5a-e, with increasing annealing temperature, the Co_3W films exhibit a similar transformation of magnetic anisotropy, which is also due to the formation of *hcp*-Co_3W phase according to the XRD result in Fig. 2b. In Fig. 5a and c, the as-deposited, 500 ºC annealed films show in-plane magnetic anisotropy. This is because these films are amorphous and their magnetic anisotropy originates from the surface anisotropy ($\Delta E = K_V V + K_S S$).[16] After annealed at 550 ºC, the film is partially crystallized and the Co_3W alloy phase forms gradually. The Co_3W phase has a large magnetocrystalline anisotropy that is compatible to the surface anisotropy and leads to a small difference between the in-plane and out-of-plane saturation fields. When the annealing temperatures rise to 600 ºC and 650 ºC, the films have almost identical in-plane and out-of-plane hysteresis loops, which means the magnetocrystalline anisotropy exceeds surface anisotropy and becomes the dominant factor. Because of the random distribution of crystal axis directions, the magnetocrystalline anisotropy axes of the completely crystallographic Co_3W films are randomly distributed. As shown in Fig. 5f, for the as-deposited and annealed Co_3W films below 600 ºC, both in-plane and out-of-plane H_C increases with the increasing annealing temperature. The film annealed at 600 ºC has the highest in-plane H_C of 512 Oe and out-of-plane H_C of 388 Oe. However, when the annealing temperature rises to 650 ºC, the in-plane H_C of the film decreases. It may be attributed that the grain boundaries in the Co_3W films become ambiguous and the interaction among the grains becomes weak. Actually, different microstructures of the Co_3W films annealed at different temperatures have been observed in Fig. 4.

From Fig. 5a, it can also be observed that the saturation magnetization (M_S) of the as-deposited Co_3W film is very small. For the sample annealed at 500 ºC, M_S reaches 176.5 emu/cm^3. However, when the annealing temperature rises from 500 ºC to 650 ºC, M_S almost

reduces linearly, while there is some distinction between the in-plane M_S and out-of-plane M_S. M_S is mainly contributed by the mean moment of Co atoms since W has a negligible induced moment. And the magnetic moment of Co atoms is decided by the number of Co first neighbors.[17] For the as-deposited film, Co and W atoms are distributed chaotically and Co atoms in the film may have less Co atoms as first neighbors, resulting in a strong reduction on magnetic moment. After the Co_3W film is annealed at 500 ºC, although it is still amorphous, atomic thermal motion gives rise to the rearrangement of Co and W atoms and thus there are more first neighbors of Co atoms, which can be proved by its large M_S. The Slater-Pauling model suggests that a gap in conduction-band density of states tends to conserve the number of conduction electrons in an alloy series leading to a linear variation of m_{at} (the mean magnetic moment per atom of the alloy) with Z_M (the atomic valence of the metal M. $Z_M = 6$ for W).[16] The relationship between m_{at} and x (at.% W) is then expressed as

$$m_{at}(x) = m_{metal} - x(10 + Z_M - Z_T)\mu_B, \qquad (8)$$

where Z_T and m_{metal} represent the atomic valence and magnetic moment in the pure T metal (Z_T = 9 and m_{metal} =1.7μB for Co). According to equation (8), the magnetic moment of Co atoms in Co_3W alloy is nearly zero, which means the M_S of Co_3W alloy is very small. Increasing annealing temperature, the film is gradually crystallized to form *hcp* Co_3W alloy, while M_S decreases almost linearly with the crystallization of Co_3W alloy.

The addition of tungsten atoms in the CoW alloys not only modifies their magnetic properties significantly, but also greatly enhances their corrosion resistance. The corrosion resistance of the Co_3W films is evaluated through measuring their H_C after immersing them in 0.5 % NaCl solution at room temperature. The as-prepared, 550 ºC annealed and 600ºC annealed Co_3W films are

chosen to be studied. Their H_C values with different immersing time have been shown in Fig. 6a. It can be observed that all the Co_3W samples only show little changes of H_C even after being immersed in 0.5 % NaCl solution for 170 h. Subsequently, XPS measurements are performed on the CoW films with different tungsten contents. Fig. 6b shows the W $4f_{7/2}$ peak of all the CoW films annealed at 600 ºC. For the CoW films with 2, 11, 18 and 26 at.% W, the W $4f_{7/2}$ peak at 31.4 eV and W $4f_{5/2}$ peak at 33.6 eV belong to tungsten metal, while the W $4f_{7/2}$ peak at 35.8 eV and W $4f_{5/2}$ peak at 37.98 eV belong to WO_3.[18] It suggests that some tungsten atoms on the surface of the CoW films have been oxidized although no obvious tungsten oxides can be observed on the XRD patterns of Fig. 2a. However, because of the ultrathin tungsten oxide layer on the surface, the inner Co_3W alloy is protected from further oxidation. The formation of the WO_3 passivation layer should be attributed to the fact that tungsten atoms are easily oxidized in air because WO_3/W has a low standard reduction potential of -0.09 V. Fig. 6c shows the Co $2p_{3/2}$ peak of the CoW films. For the film with 2 at.% W, the Co $2p_{3/2}$ peak at 778.3 eV and Co $2p_{1/2}$ peak at 793 eV of Co metal are very weak, while the Co $2p_{3/2}$ peak at 780.4 eV and Co $2p_{1/2}$ peak at 795.6 eV of CoO have relatively strong intensities.[19] It indicates that the Co atoms on the surface of the films almost have been completely oxidized. However, when the tungsten content in the CoW films increases from 11 at.% to 26 at.%, the intensity of the Co $2p_{3/2}$ peak of Co metal increases following the reduced intensity of the Co $2p_{3/2}$ peak of CoO. It can be concluded that the tungsten atoms in the CoW alloys helps to reduce the oxidation of Co atoms and therefore enhance their corrosion-resistance. For the CoW film with 26 at.% W, the W $4f_{7/2}$ peak occurs at 30.98 eV, shifting to higher binding energy upon forming Co alloys compared to the W $4f_{7/2}$ peak at 30.89 eV for the CoW film with 11 at.% W. The result is similar with the XPS result of some other

Co-based alloys.[20] The excellent corrosion-resistance properties make the Co_3W alloy films very promising in practical applications.

4. Conclusions

A series of CoW films have been fabricated by electrochemical deposition method. Their compositions can be modified by adjusting electrolyte concentrations, pH values and applied potentials. The effects of the composition and annealing temperature on the structural and magnetic properties of the CoW films were studied. When either the tungsten content or annealing temperature is low, the CoW films exhibit in-plane anisotropy because the surface anisotropy is dominated. When the hard ferromagnetic Co_3W phase forms completely, the CoW films become isotropic because their magnetocrystalline anisotropy exceeds the surface anisotropy. The corrosion-resistance of the Co_3W films is also studied. After being immersed in 0.5% NaCl solution for 170 h, the as-prepared and annealed Co_3W films have no dramatic change of the magnetic properties, which means the Co_3W films have excellent corrosion-resistance property. Theoretical analysis and XPS measurement suggest that the corrosion-resistance originates from the tungsten oxide passivation layer on the surface of the films.

Acknowledgment

This work was partially supported by the National Basic Research Program of China (Grant No. 2012CB932702), the National Science Foundation of China (Grant Nos. 11174031, 51371024, 51325101, 51271020), PCSIRT, Beijing Nova program (Grant no. 2011031), the Fundamental Research Funds for the Central Universities.

References

1 N. Tsyntsaru, H. Cesiulis, M. Donten, J. Sort, E. Pellicer and E. J. Podlaha-Murphy, *Surf. Engin.*

Appl. Electrochem., 2012, **48**, 491-520.

2 N. Sulitanu and F. Brinza, *J. Optoelectron. Adv. Mater.*, 2003, **5**, 421-427.

3 N. V. Myung, D. -Y. Park, B. -Y. Yoo and P. T. A. Sumodjo, *J. Magn. Magn. Mater.*, 2003, **265**, 189-198.

4 M. P. Marceta Kaninski, S. M. Miulovic, G. S. Tasic, A. D. Maksic and V. M. Nikolic, *Int. J. Hydrogen Energy*, 2011, **36**, 5227-5235.

5 J. -J. Wang, Y. Tan, C.-M. Liu and O. Kitakami, *J. Magn. Magn. Mater.*, 2013, **334**, 119-123.

6 M. Glushkova, T. Bairachna, M. Vedand and M. Sakhnenko, *Mater. Res. Soc. Symp. Proc.*, 2012, **1491**, 10.1557.

7 E. Lassner and W. D. Schubert, *Tungsten: properties, chemistry, technology of the element, alloys, and chemical compounds*, Springer, 1999.

8 O. Younes and E. Gileadi, *J. Electrochem. Soc.*, 2002, **149**, C100-C111.

9 O. Younes-Metzler, L. Zhu and E. Gileadi, *Electrochim. Acta*, 2003, **48**, 2551-2562.

10 U. Admon and M. P. Dariel, *J. Appl. Phys.*, 1987, **62**, 1943-1947.

11 H. Capel, P. H. Shipway and S. J. Harris, *Wear*, 2003, **255**, 917-923.

12 E. V. Pustovalov, E. B. Modin, O. V. Voitenko, A. N. Fedorets, A. V. Dubinets, B. N. Grudin, V. S. Plotnikov and S. S. Grabchikov, *Nanoscale Res. Lett.*, 2014, **9**, 405-409, 66-73.

13 S. M. S. I. Dulal, H. J. Yun, C. B. Shin and C. -K. Kim, *Electrochim. Acta*, 2007, **53**, 934-943.

14 S. S. Belevskii, N. I. Tsyntsaru and A. I. Dikusar, *Surf. Engin. Appl. Electrochem.*, 2010, **46**, 91-99.

15 H. Cesiulis, A. Baltutiene, M. Donten and Z. Stojek, *J. Solid State Electrochem.*, 2002, **6**, 237-244.

16 F. Tournus, A. Tamion, N. Blanc, A. Hannour, L. Bardotti, B. Prével, P. Ohresser, E. Bonet, T. Epicier and V. Dupuis, *Phys. Rev. B*, 2008, **77**, 144411.

17 A. I. Figueroa, J. Bartolomé, L. M. García, F. Bartolomé, C. Magén, A. Ibarra, L. Ruiz, J. M. González-Calbet, F. Petroff, C. Deranlot, S. Pascarelli, P. Bencok, N. B. Brookes, F. Wilhelm and A. Rogalev, *Phys. Rev. B*, 2011, **84**, 184423.

18 X. P. Wang, B. Q. Yang, H. X. Zhang and P. X. Feng, *Nanoscale Res. Lett.*, 2007, **2**, 405-409.

19 I. G. Casella and M. R.Guascito, *J. Electroanal. Chem.*, 1999, **476**, 54-63.

20 G. Chen, D. Xia, Z. Nie, Z. Wang, L. Wang, L. Zhang and J. Zhang, *Chem. Mater.*, 2007, **19**, 1840-1844.

Figures Captions:

Table 1 The W content and the deposition parameters. There are 0.1 $mol \cdot L^{-1}$ of $CoSO_4$ and 0.2 $mol \cdot L^{-1}$ Na_3Cit in every solution.

Fig. 1 Cyclic voltammograms for the solutions with different pH values.

Fig. 2 (a) XRD patterns of the CoW films with different compositions annealed at 600 ºC for 30 min in vacuum. (b) XRD patterns of the CoW films with 26 at.% W(Co_3W) annealed at different temperatures for 30 min in vacuum.

Fig. 3 SEM micrographs of the 26 at.% W (Co_3W) films. (a) as-deposited; (b) 500 ºC annealed; (c) 550 ºC annealed; (d) 600 ºC annealed; (e) 650 ºC annealed. (f) EDS of the as-deposited Co_3W film.

Fig. 4 Hysteresis loops of the CoW films with different tungsten contents. (a) 2 at.% W, (b) 11 at.% W, (c) 18 at.% W, (d) 20 at.% W, (e) 26 at.% W. (f) Dependence of H_C and M_r/M_S of the CoW films on the tungsten content. All the samples have been annealed at 600 ºC for 30 min in vacuum.

Fig. 5 (a)-(e) Hysteresis loops of the Co_3W films annealed at different temperatures for 30 min. (f) H_C of the Co_3W films as a function of the annealing temperature.

Fig. 6 (a) H_C of the Co_3W films with different immersing time in the 0.5% NaCl solution. The XPS spectra for W 4f peaks (b) and Co 2p peaks (c) of the CoW films with different tungsten contents.

Table 1. (Lina Yu et al.):

Tungsten content (at.% W)	Na_2WO_4 ($mol \cdot L^{-1}$)	pH	Potentials (V vs. Ag/AgCl)
pH-dependent experiment			
11	0.5	***6.0***	-1.0
14	0.5	***6.5***	-1.0
17	0.5	***7.0***	-1.0
19	0.5	***8.0***	-1.0
Potential-dependent experiment			
9	0.5	6.5	***-2.0***
15	0.5	6.5	***-1.5***
26	0.5	6.5	***-1.0***
WO_4^{2-}-dependent experiment			
14	***0.05***	6.5	-1.0
17	***0.1***	6.5	-1.0
18	***0.2***	6.5	-1.0
20	***0.3***	6.5	-1.0
20	***0.4***	6.5	-1.0

Fig. 1. (Lina Yu et al.):

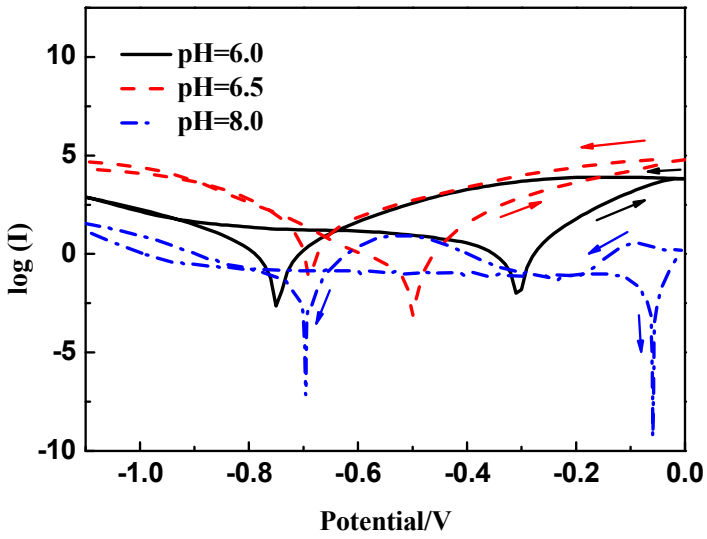

Fig. 2. (Lina Yu et al.):

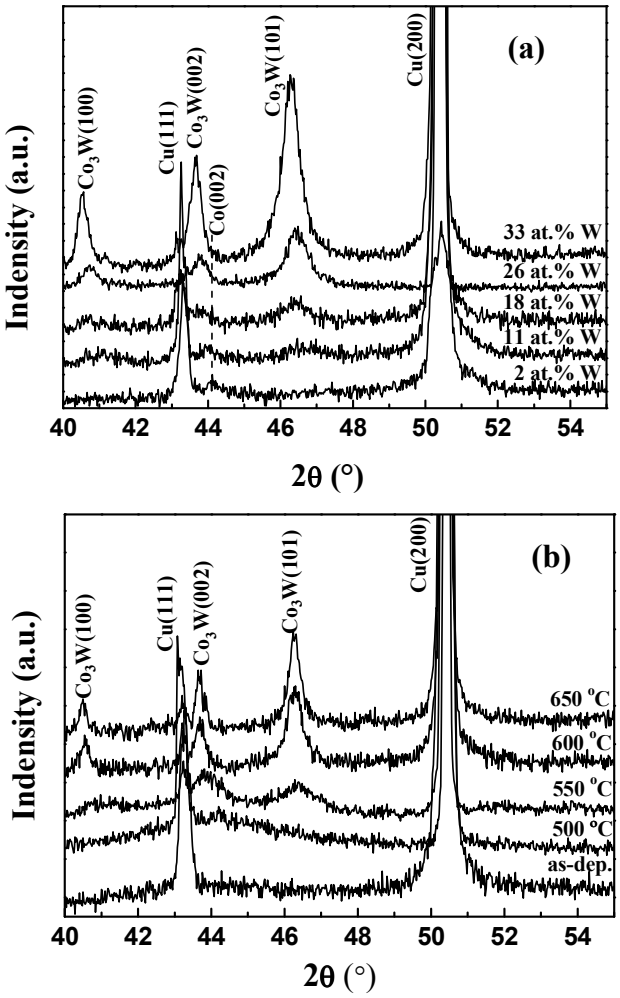

Fig. 3. (Lina Yu et al.):

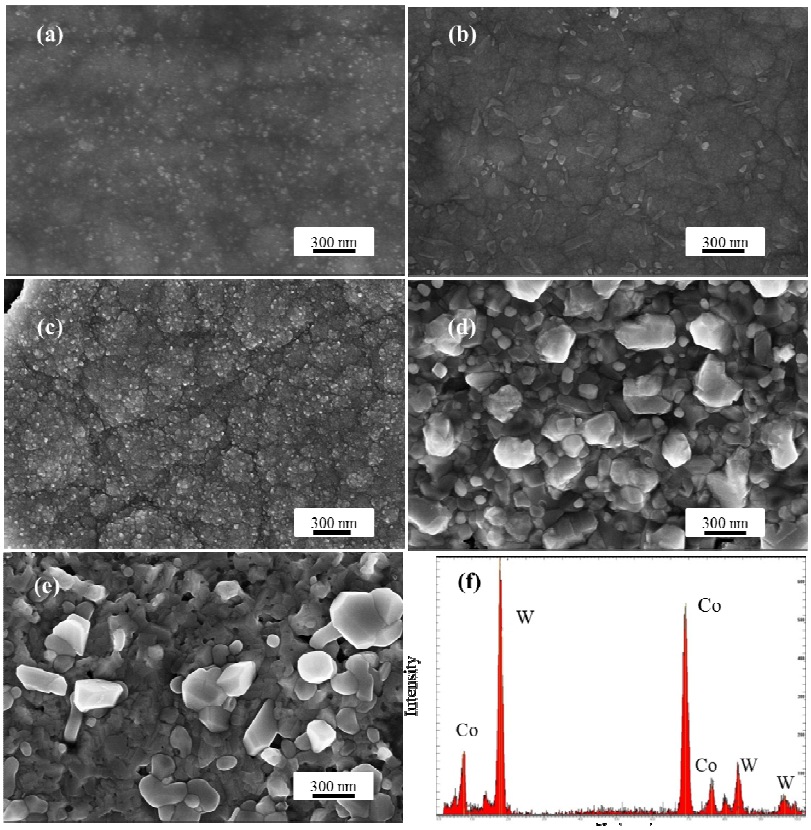

Fig. 4. (Lina Yu et al.):

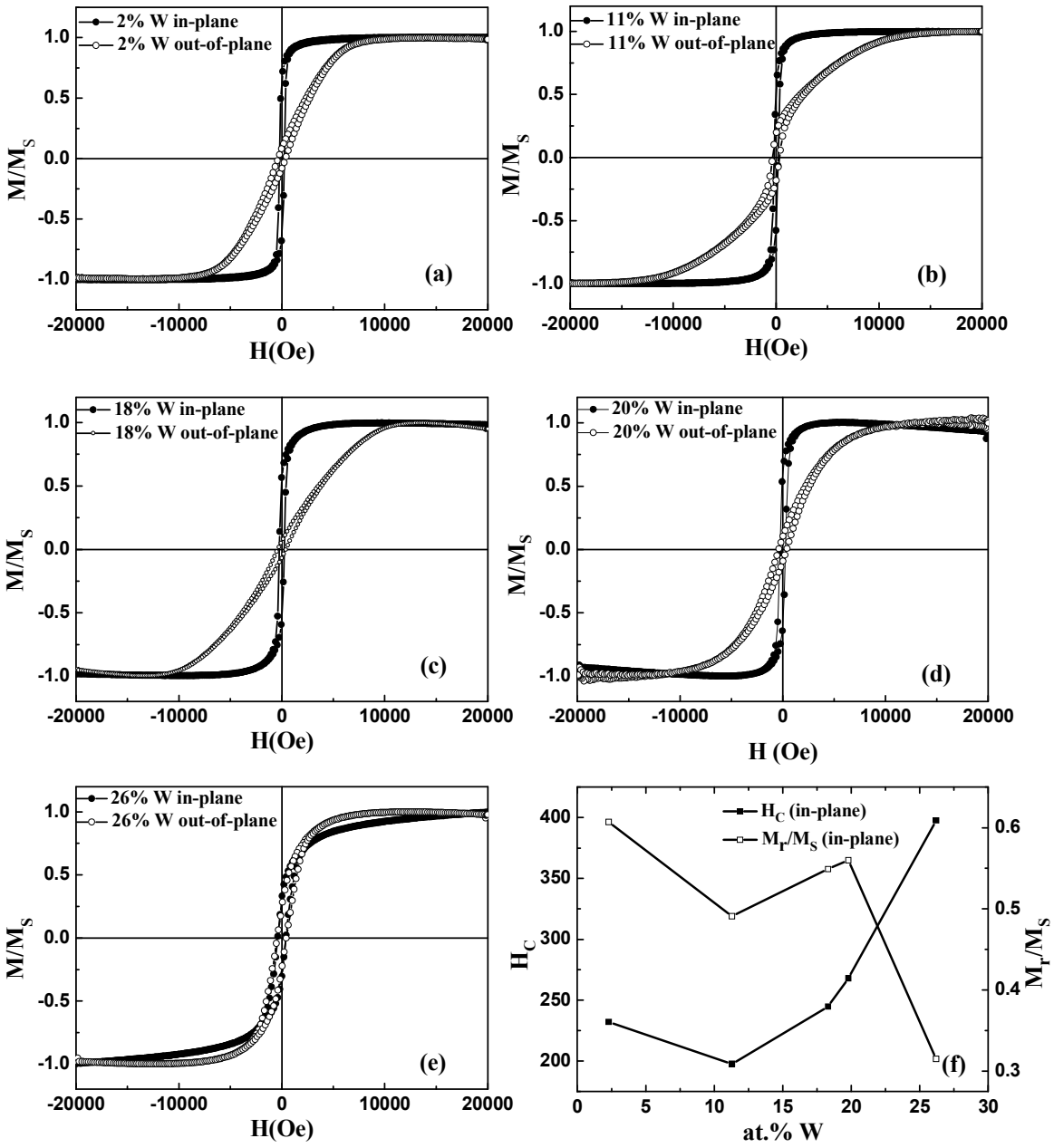

Fig. 6. (Lina Yu et al.):

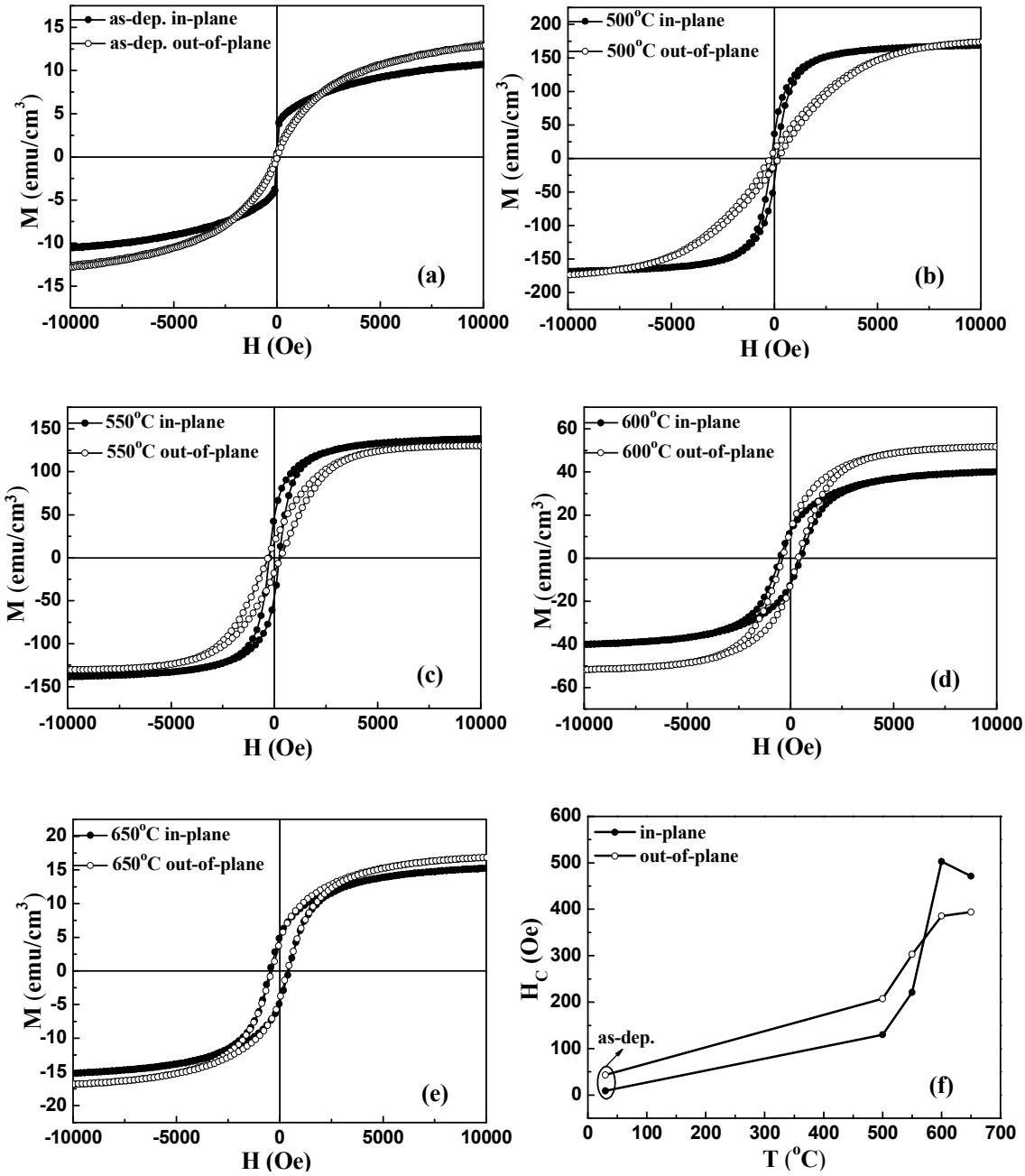

Fig. 6. (Lina Yu et al.):

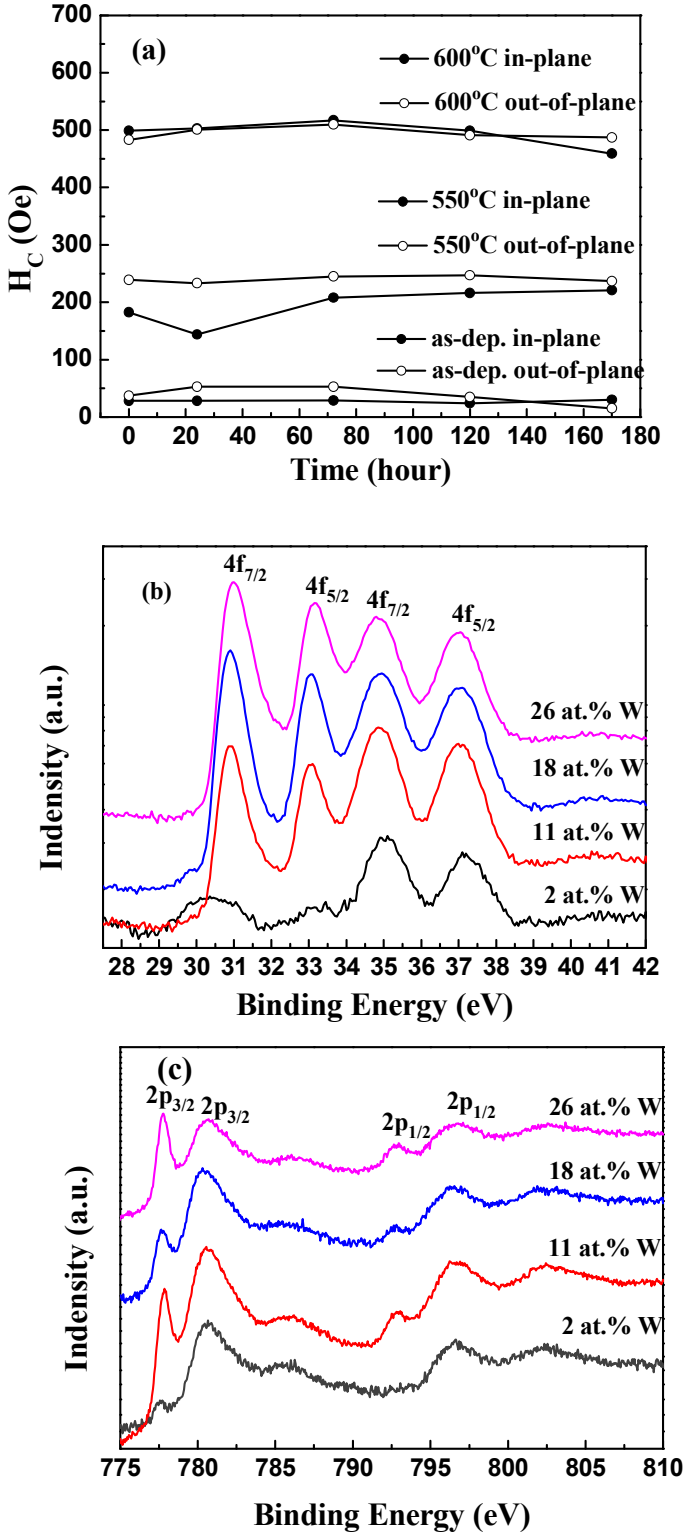

Unable to Convert Image

The dimensions of this image (in pixels) are too large to be converted. For this image to convert, the total number of pixels (height x width) must be less than 40,000,000 (40 megapixels).

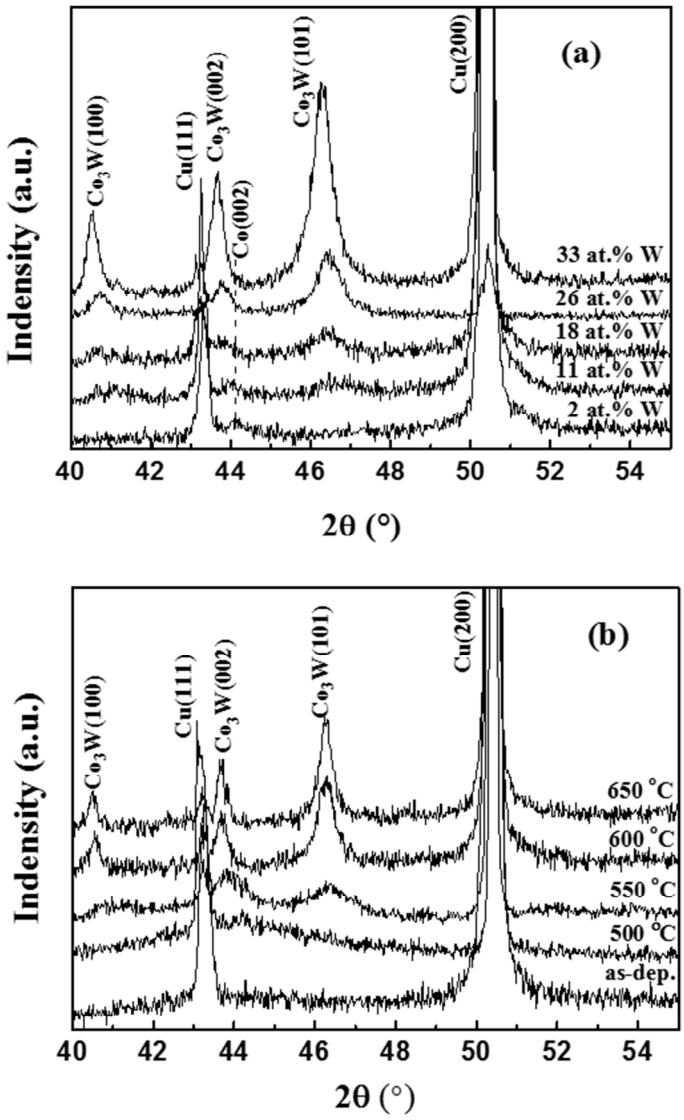

152x206mm (600 x 600 DPI)

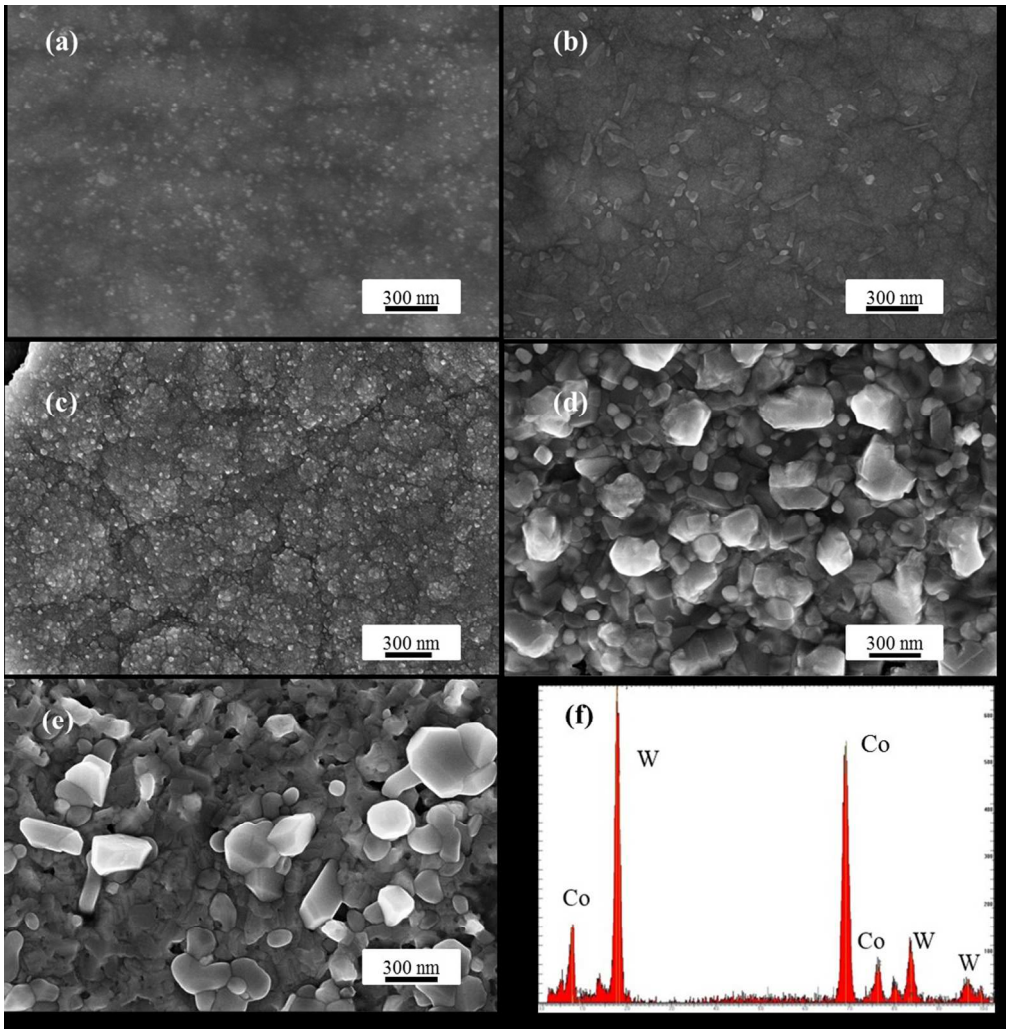

195x199mm (300 x 300 DPI)

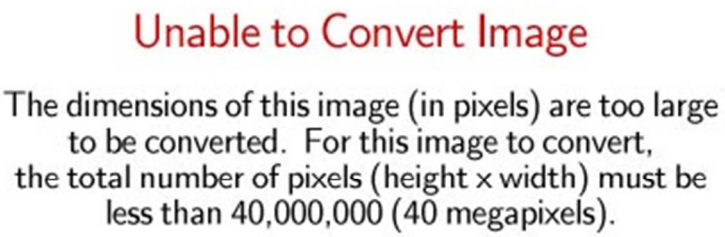

Unable to Convert Image

The dimensions of this image (in pixels) are too large to be converted. For this image to convert, the total number of pixels (height x width) must be less than 40,000,000 (40 megapixels).

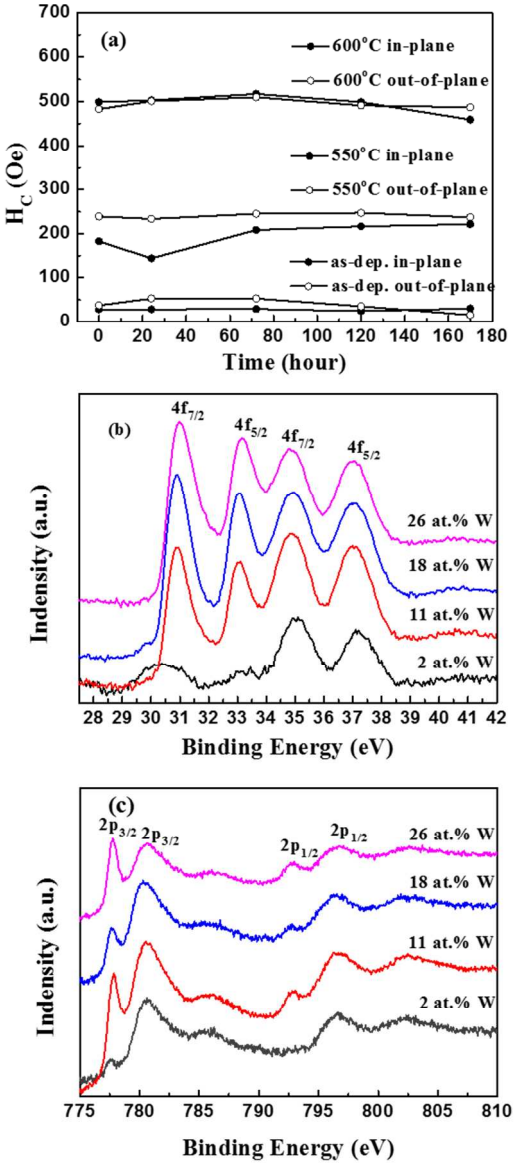

219x429mm (600 x 600 DPI)

Tungsten content (at.% W)	Na_2WO_4 ($mol \cdot L^{-1}$)	pH	Potentials (V vs. Ag/AgCl)
pH-dependent experiment			
11	0.5	***6.0***	-1.0
14	0.5	***6.5***	-1.0
17	0.5	***7.0***	-1.0
19	0.5	***8.0***	-1.0
Potential-dependent experiment			
9	0.5	6.5	***-2.0***
15	0.5	6.5	***-1.5***
26	0.5	6.5	***-1.0***
WO_4^{2-}-dependent experiment			
14	***0.05***	6.5	-1.0
17	***0.1***	6.5	-1.0
18	***0.2***	6.5	-1.0
20	***0.3***	6.5	-1.0
20	***0.4***	6.5	-1.0

Table 1 The W content and the deposition parameters. There are 0.1 mol•L-1 of CoSO4 and 0.2 mol•L-1 Na3Cit in every solution.
338x243mm (96 x 96 DPI)